The Journal of Chemical Physics

RESEARCH ARTICLE | JUNE 05 2023

Spin-velocity locking in a helical chain of atomic $p_{\pm}$ orbitals

Special Collection: Chiral Induced Spin Selectivity

Shinnosuke Kashiwa; Hiroshi Akera

J. Chem. Phys. 158, 214705 (2023)
https://doi.org/10.1063/5.0152103

The Journal of Chemical Physics ARTICLE scitation.org/journal/jcp

Spin-velocity locking in a helical chain of atomic $p_\pm$ orbitals

Cite as: J. Chem. Phys. 158, 214705 (2023); doi: 10.1063/5.0152103
Submitted: 27 March 2023 • Accepted: 16 May 2023 •
Published Online: 5 June 2023

Shinnosuke Kashiwa[1] and Hiroshi Akera[2,a)]

AFFILIATIONS

[1] Division of Applied Physics, Graduate School of Engineering, Hokkaido University, Sapporo, Hokkaido 060-8628, Japan
[2] Division of Applied Physics, Faculty of Engineering, Hokkaido University, Sapporo, Hokkaido 060-8628, Japan

Note: This paper is part of the JCP Special Topic on Chiral Induced Spin Selectivity.
[a)]**Author to whom correspondence should be addressed:** akera@eng.hokudai.ac.jp

ABSTRACT

Observations of a high spin selectivity in various helical structures, which is called the chirality-induced spin selectivity, suggest a common mechanism originating from the helical geometry. In this paper, we consider a helical chain of atomic $p_\pm$ orbitals having the tangential angular momentum $l = \pm 1$. We show in this model that the coupling of l and the spin gives rise to spin-velocity locking, i.e., directions of spin and group velocity are parallel or antiparallel depending on the chirality of the helix, and consequently, an almost perfect spin selectivity in a specific energy region in a wide range of the curvature and the torsion of the helix. We find that the present spin-velocity locking originates from the helical symmetry in which the Hamiltonian is invariant with respect to a combined operation of the rotation around the helix axis and the translation along the helix axis. Therefore, we expect that spin-velocity locking occurs in a wide variety of helical structures.

I. INTRODUCTION

Spin polarization, which is used in spintronics, is generated in nonmagnetic materials by the spin–orbit interaction (SOI) in the spin Hall effect and the current-induced spin polarization. To efficiently generate spin polarization, materials with heavy elements having large SOI have been employed. Recently, however, in various helical organic molecules[1–10] consisting of light elements with small SOI at room temperature, the chirality-induced spin selectivity (CISS) (see, for a review, Ref. 11) has been observed in which electrons conduct much more easily when orientations (along the helix axis) of spin and transport are the same or opposite depending on the chirality of the structure. The CISS has also been observed in chiral inorganic crystals.[12]

To understand the mechanism for the high spin selectivity despite small SOI, many theoretical attempts have been made. Among others, spin-velocity locking, in which orientations (along the helix axis) of spin and group velocity are the same or opposite depending on the chirality of the helix, has been proposed for the mechanism of CISS by Michaeli and Naaman.[13] It is derived in a helical tube continuum model and occurs in a specific energy range. To obtain a high spin selectivity through spin-velocity locking, the temperature must be low enough that the electron transport takes place within the locking energy range of the order of the SOI. Nevertheless, spin-velocity locking in a nonmagnetic one-dimensional system is an attractive feature, and its observation in a real helical system is desired. In a step toward real systems is a tight-binding model of a helical atomic chain with atomic p orbitals and the intra-atomic SOI.[14–17] Utsumi *et al.*[15] have shown in this model that spin-velocity locking occurs in a particular structure with no torsion.

In this paper, as a next step toward the observation in real systems, we explore the occurrence of spin-velocity locking in a helical atomic chain in the full parameter space of the curvature κ and the torsion τ both of which define the helix. We calculate the energy and the spin expectation value of eigenstates in a tight-binding model with the intra-atomic SOI.[14–17] We take into account atomic $p_\pm$ orbitals with the tangential angular momentum $l = \pm 1$ and neglect p_0 orbital with $l = 0$ because spin-velocity locking in both the tube model[13] and the atomic model[15] has been found in energy bands that are formed from orbitals with $l = \pm 1$. In this paper, we take into account the helical symmetry of the atomic chain, which reduces the number of eigenstates to four at each value of Θ, the dimensionless quantity conserved in the helical symmetry.

We find that the present helical atomic chains exhibit spin-velocity locking in two separate regions of the structure parameter

space, a torsion-dominant region ($\tau > \kappa$) and a curvature-dominant region ($\kappa > \tau$), where we identify different types of the locking, which we call type I and type II locking, respectively. In both types, the locking occurs because the SOI opens an energy gap at the intersection between opposite-spin and opposite-velocity channels. The difference between type I and type II is in the orbital character of these channels. In the torsion-dominant type I region, the two channels have the same orbital character, whereas, in the curvature-dominant type II region, they have different orbital characters. We show that in both types, the velocity change simultaneously occurring with the SOI-induced spin flip is ensured by the conservation of Θ in the helical symmetry.

II. MODEL AND HAMILTONIAN

We consider an atomic chain that is placed along a helix with equal distances (d) between neighboring atoms (Fig. 1). By choosing the z axis along the helix axis, coordinates of the nth atom ($n = \ldots, 0, 1, 2, \ldots$) are

$$(x_n, y_n, z_n) = (a\cos n\varphi, a\sin n\varphi, bn\varphi), \tag{1}$$

in which $a(>0)$ is the radius, and $2\pi|b|$ is the pitch of the helix. The increment of the angle around the z axis is $\varphi(>0)$. We consider general helical atomic chains in which the number of atoms per pitch, $2\pi/\varphi$, is not restricted to be an integer. The sign of b determines the chirality. In the following, we only consider the chirality of $b > 0$.

In the presence of the helical symmetry of the chain, the Hamiltonian $\hat{H}$ is invariant with respect to the operation $\hat{S} = \hat{T}\hat{R}$ where $\hat{R}$ is the rotation by φ around the z axis, and $\hat{T}$ is the translation by $b\varphi$ along the z axis. Owing to this invariance, i.e., $\hat{S}\hat{H}\hat{S}^{-1} = \hat{H}$, each eigenvector of $\hat{H}$, which we denote by $|\psi\rangle$, can be chosen to satisfy $\hat{S}|\psi\rangle = \exp(-i\Theta)|\psi\rangle$. Here, $\hbar\Theta$ consists of the z component of the angular momentum (including spin and orbital components) multiplied by the angle φ and the z component of the linear momentum multiplied by the translation $b\varphi$.

In each atom, we take into account $\mathrm{p}_{\hat{n}}$ and $\mathrm{p}_{\hat{b}}$ orbitals in the normal and binormal directions, respectively, of the helix (Fig. 1), which are related to $|\mathrm{p}_l\rangle = (|\mathrm{p}_{\hat{n}}\rangle + il|\mathrm{p}_{\hat{b}}\rangle)/\sqrt{2}$ having the angular momentum $l = \pm 1$ in the tangential direction. We neglect the $\mathrm{p}_{\hat{t}}$ orbital in the tangential direction by separating it from $\mathrm{p}_{\hat{n}}$ and $\mathrm{p}_{\hat{b}}$ in energy with a crystal field.[15,16] Then, basis vectors satisfying $\hat{S}|\psi\rangle = \exp(-i\Theta)|\psi\rangle$ are expressed by[18]

$$|\mathrm{p}_\alpha\sigma\Theta\rangle = \frac{1}{\sqrt{N}}\sum_n \exp(i\Theta n)\hat{S}^n|\mathrm{p}_\alpha\sigma\rangle. \tag{2}$$

Here, N is the number of atoms in the chain, $|\mathrm{p}_\alpha\sigma\rangle = |\mathrm{p}_\alpha\rangle|\sigma\rangle$, $|\mathrm{p}_\alpha\rangle$ expresses p_α orbitals ($\alpha = \hat{n}, \hat{b}$) of the $n = 0$ atom, and $\hat{\sigma}_z|\sigma\rangle = \sigma|\sigma\rangle$ in which $\hat{\boldsymbol{\sigma}} = (\hat{\sigma}_x, \hat{\sigma}_y, \hat{\sigma}_z)$ is the Pauli spin operator and $\sigma = \pm 1$. We have, for the spin,

$$\hat{S}|\sigma\rangle = \hat{R}|\sigma\rangle = \exp(-i\varphi\sigma/2)|\sigma\rangle. \tag{3}$$

Our Hamiltonian consists of two terms,

$$\hat{H} = \hat{H}_{\mathrm{hop}} + \hat{H}_{\mathrm{so}}. \tag{4}$$

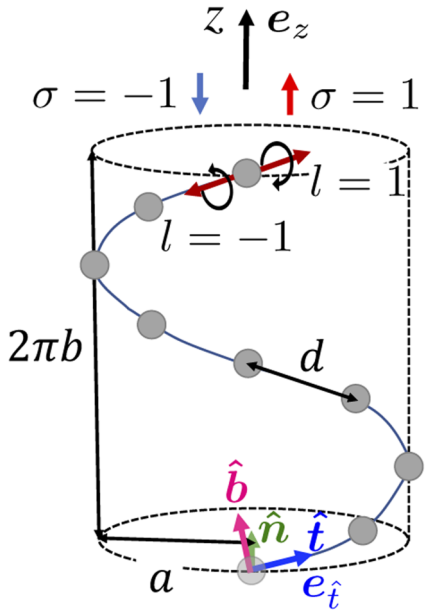

FIG. 1. An atomic chain along the helix with radius a and pitch $2\pi b$. The interatomic distance is d, and the angle around the helix axis (the z axis) between neighboring atoms is φ. This paper considers general helical atomic chains in which the number of atoms per pitch is not restricted to be an integer. The z component of the spin $s_z = \sigma/2$ ($\sigma = \pm 1$), and the tangential components of the atomic orbital angular momentum $l_{\hat{t}} = l$ ($l = \pm 1$) are used to define basis vectors. Also indicated are the tangential, normal, and binormal directions, which are denoted by $\hat{t}$, $\hat{n}$, and $\hat{b}$. Unit vectors $\boldsymbol{e}_{\hat{t}}$ and $\boldsymbol{e}_z$ are in the $\hat{t}$ and z directions, respectively.

The first term $\hat{H}_{\mathrm{hop}}$ describes the hopping between the nearest neighbor atoms,

$$\hat{H}_{\mathrm{hop}} = \sum_{\alpha',\alpha=\hat{n},\hat{b}}\sum_n t_{n+1,n}^{\alpha'\alpha}|\mathrm{p}_{\alpha'}n+1\rangle\langle\mathrm{p}_\alpha n| + \mathrm{h.c.}, \tag{5}$$

where $|\mathrm{p}_\alpha n\rangle = \hat{S}^n|\mathrm{p}_\alpha\rangle$ and h.c. denote the Hermitian conjugate of the preceding term. The hopping matrix element $t_{n+1,n}^{\alpha'\alpha} = \langle\mathrm{p}_{\alpha'}n+1|\hat{H}_{\mathrm{hop}}|\mathrm{p}_\alpha n\rangle$ is evaluated by using the formula[19] that expresses the hopping matrix element between p orbitals of arbitrary directions belonging to two atoms at any positions with the use of Slater-Koster parameters,[20] $V_{\mathrm{pp}\pi}$ and $V_{\mathrm{pp}\sigma}$, which we simply denote by V_π and V_σ. The second term $\hat{H}_{\mathrm{so}}$ expresses the intra-atomic SOI and is given, in the present model, with $\mathrm{p}_{\hat{n}}$ and $\mathrm{p}_{\hat{b}}$, by

$$\hat{H}_{\mathrm{so}} = \sum_n \lambda_{\mathrm{so}}\hat{L}_{\hat{t}n}\hat{\sigma}_{\hat{t}n}/2, \tag{6}$$

where $\hat{L}_{\hat{t}n} = \hat{\boldsymbol{L}}_n \cdot \boldsymbol{e}_{\hat{t}n}$, with $\hbar\hat{\boldsymbol{L}}_n$ the orbital angular momentum operator with respect to (x_n, y_n, z_n) and $\boldsymbol{e}_{\hat{t}n}$ the unit vector in the tangential direction at (x_n, y_n, z_n), and $\hat{\sigma}_{\hat{t}n} = \hat{\boldsymbol{\sigma}} \cdot \boldsymbol{e}_{\hat{t}n}$. In the matrix elements $\langle\mathrm{p}_{\hat{b}}n'|\hat{L}_{\hat{t}n}|\mathrm{p}_{\hat{n}}n''\rangle$, we only consider those with $n' = n = n''$.

We derive eigenstates of the Hamiltonian, $\hat{H}$, in Eq. (4) by expressing each eigenvector in a linear combination of basis vectors in Eq. (2). We describe procedures to calculate the energy, the group velocity, and the spin expectation value of eigenstates in Appendix.

III. SPIN-VELOCITY LOCKING

A. Eigenstates: Energy and spin expectation value

Figure 2 presents the energy and the spin expectation value of each eigenstate as a function of Θ in the vicinity of the energy band bottom in a helical carbon chain with $\kappa d = 0.1$ and $\tau d = 0.1$, where κ and τ are the curvature and the torsion defined by

$$\kappa = \frac{a}{a^2 + b^2}, \qquad \tau = \frac{b}{a^2 + b^2}. \tag{7}$$

In the calculation, we have used values of the Slater-Koster parameters $V_\pi = -2.97$ eV and $V_\sigma = 7.43$ eV (calculated using the formula in Ref. 21 into which we have substituted $S_{ij} = 0$ and $R_{ij} = 1.266$ Å the value in the first-principles calculation[22] of the interatomic distance in a straight linear carbon chain) and that of the atomic SOI parameter $\lambda_{so} = 0.006$ eV (from Ref. 23).

In the highlighted energy region of Fig. 2 (upper panel), avoided-crossings occur around $\Theta = \pm 0.1$ due to the SOI [solid (dotted) lines indicate energy bands in the presence (absence) of the SOI], and four transport channels (dotted lines), which existed in the absence of the SOI, are eliminated. The remaining channels with spin orienting in the positive z direction ($\sigma = \uparrow$) at $\Theta = 0.05$ and 0.25 have the group velocity in the positive z direction since $\partial E/\partial\Theta > 0$, whereas those with $\sigma = \downarrow$ at $\Theta = -0.05$ and -0.25 have $\partial E/\partial\Theta < 0$. Therefore, spin-velocity locking occurs in the highlighted energy region. To evaluate the spin selectivity, we calculate the conductance of each spin component in the absence of scatterings at absolute zero by employing the Landauer formula

$$G_\sigma = \frac{e^2}{h} \sum_{\nu\Theta(v>0)} \langle \nu\Theta|\sigma\rangle\langle\sigma|\nu\Theta\rangle, \tag{8}$$

where the summation is taken over eigenstates $|\nu\Theta\rangle$ (ν: band index) with positive velocity at energy E. Figure 3 shows that in the energy region of the spin-velocity locking, $(G_\uparrow - G_\downarrow)/(G_\uparrow + G_\downarrow) \approx 0.998$. Therefore, the spin selectivity is almost perfect.

We find in Fig. 2 that spin-velocity locking occurs because an energy gap opens at the intersection between opposite-spin channels due to the SOI that mixes $\sigma = \uparrow$ and $\sigma = \downarrow$ states. The magnitude of the SOI-induced gap is proportional to $|\langle\uparrow|\hat{\sigma}_{\hat{t}n}|\downarrow\rangle|$ and, therefore, vanishes at $\kappa \to 0$ ($a \to 0$).

Figure 4 presents another helical structure ($\kappa d = 0.2$ and $\tau d = 0.01$) that exhibits the spin-velocity locking. The major difference between spin-velocity locking in Figs. 2 and 4 is clearly seen in the energy band in the absence of the SOI (dotted line). In Fig. 2, the SOI-induced gap opens between same-orbital channels (we call this type I), whereas in Fig. 4, it opens between different-orbital channels (type II).

Every spin-velocity locking in our model is classified into type I and type II. Type I and type II regions in the κ-τ plane are shown in Fig. 5 at $V_\sigma/V_\pi = -2.50$ (of carbon) and -4.15 (of iodine in which values of $V_\pi = -0.55$ eV and $V_\sigma = 2.28$ eV were obtained in Ref. 24 by fitting tight-binding energy bands of a straight linear iodine chain to those in the first-principles calculation). In evaluating type I and type II regions in Fig. 5, we have assumed the infinitesimal SOI ($\lambda_{so} \to 0$) for simplicity.

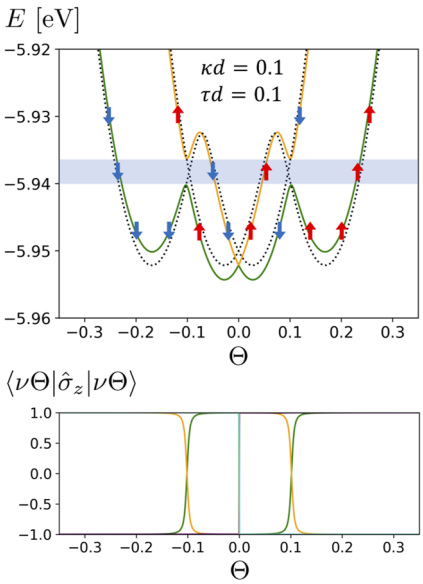

FIG. 2. Type I locking at $\kappa d = 0.1$ and $\tau d = 0.1$. Here, $\kappa = a/(a^2 + b^2)$ and $\tau = b/(a^2 + b^2)$ are the curvature and the torsion, respectively, of the helix. The upper panel plots the energy E of each eigenstate in the vicinity of the band bottom (two eigenstates out of four appear in the plot) as a function of the dimensionless quantity conserved in the helical symmetry Θ. The lower panel plots the expectation value of $\hat{\sigma}_z$ with respect to each eigenstate. Each band is characterized by the value of $\sigma(=\uparrow,\downarrow)$ except in the neighborhood of anti-crossing points. In the highlighted energy region, spin-velocity locking is realized (see text). Dotted lines show the energy in the absence of the SOI.

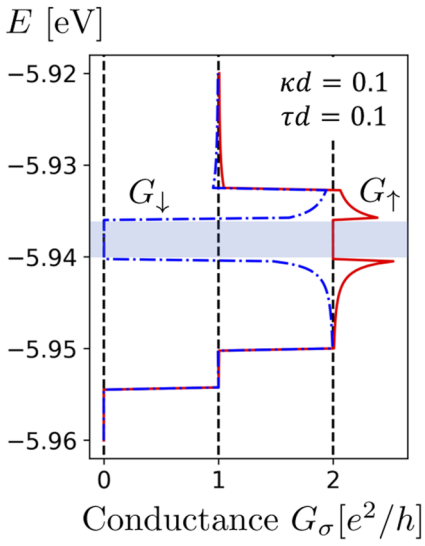

FIG. 3. Conductance in the Landauer formula of spin σ component in the absence of scatterings at absolute zero is plotted as a function of energy. In the highlighted energy region of the spin-velocity locking, $(G_\uparrow - G_\downarrow)/(G_\uparrow + G_\downarrow) \approx 0.998$.

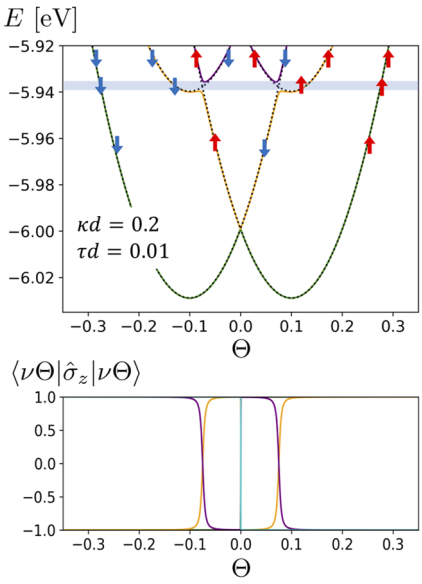

FIG. 4. Type II locking at $\kappa d = 0.2$ and $\tau d = 0.01$.

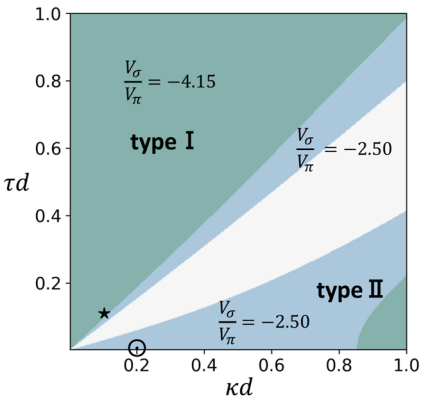

FIG. 5. Region of type I and type II spin-velocity locking (evaluated at the infinitesimal SOI, for simplicity) in the space of the curvature κ and the torsion τ multiplied by the interatomic distance d. Light and dark shades indicate spin-velocity locking at $V_\sigma/V_\pi = -2.50$ and $V_\sigma/V_\pi = -4.15$ corresponding to carbon and iodine, respectively ($V_\sigma/V_\pi = -2.50$ region includes the $V_\sigma/V_\pi = -4.15$ region). Energy and spin expectation values at $V_\sigma/V_\pi = -2.50$ of the structure indicated by ⋆ and ⊙ are presented in Figs. 2 and 4, respectively.

B. Approximate eigenstates in the absence of the SOI at $\varphi \ll 1$

In order to approach the origin of the spin-velocity locking, we derive analytical expressions of eigenvectors and eigenenergies that are approximately correct when $\varphi \ll 1$ (large helix with $\sqrt{a^2+b^2} \gg d$) in the absence of the SOI. When the SOI is absent, the Hamiltonian $\hat{H}$ in Eq. (4) reduces to $\hat{H}_{\rm hop}$ in Eq. (5), which is given by

$$\hat{H}_{\rm hop} = \sum_{\Theta}\sum_{\sigma=\pm1}\Big[2\cos\Big(\Theta-\frac{\sigma}{2}\varphi\Big)\big(t_{\hat{n}\hat{n}}|\mathrm{p}_{\hat{n}}\sigma\Theta\rangle \times\langle\mathrm{p}_{\hat{n}}\sigma\Theta| + t_{\hat{b}\hat{b}}|\mathrm{p}_{\hat{b}}\sigma\Theta\rangle\langle\mathrm{p}_{\hat{b}}\sigma\Theta|\big) - 2t_{\hat{n}\hat{b}}\sin\Big(\Theta-\frac{\sigma}{2}\varphi\Big)\big(i|\mathrm{p}_{\hat{n}}\sigma\Theta\rangle\langle\mathrm{p}_{\hat{b}}\sigma\Theta| + \mathrm{h.c.}\big)\Big]. \quad (9)$$

When $\varphi \ll 1$, the hopping matrix elements are given, up to the second order of φ, by

$$t_{\hat{n}\hat{n}} \equiv t^{\hat{n}\hat{n}}_{n+1,n} = \Big[1-\frac{(\tau d)^2}{2}\Big]V_\pi - \frac{(\kappa d)^2}{4}(V_\pi+V_\sigma),$$
$$t_{\hat{b}\hat{b}} \equiv t^{\hat{b}\hat{b}}_{n+1,n} = \Big[1-\frac{(\tau d)^2}{2}\Big]V_\pi, \quad (10)$$
$$t_{\hat{n}\hat{b}} \equiv t^{\hat{n}\hat{b}}_{n+1,n} = \tau d\, V_\pi = -t^{\hat{b}\hat{n}}_{n+1,n}.$$

1. At $\kappa \ll \tau, \varphi \ll 1$ in type I region

Within the region of small φ ($\varphi \approx \sqrt{(\kappa d)^2+(\tau d)^2}$ at $\varphi \ll 1$), we separately investigate the region with $\kappa \ll \tau$ ($a \ll b$) and that with $\tau \ll \kappa$ ($b \ll a$). First, we assume that $\kappa \ll \tau$ in addition to $\varphi \ll 1$. Then, we obtain, from Eqs. (9) and (10), approximate eigenvectors and eigenenergies at $\Theta \sim \varphi$

$$|\mathrm{p}_l\sigma\Theta\rangle = \frac{1}{\sqrt{2}}(|\mathrm{p}_{\hat{n}}\sigma\Theta\rangle + il|\mathrm{p}_{\hat{b}}\sigma\Theta\rangle), \quad (11)$$

$$E_{l\sigma}(\Theta) = 2V_\pi\cos\Big(\Theta - l_z\varphi - \frac{\sigma}{2}\varphi\Big), \quad (12)$$

with

$$l_z = l\,\boldsymbol{e}_{\hat{t}0}\cdot\boldsymbol{e}_z = l\cos\theta \quad (l=\pm1), \quad (13)$$

where θ is the angle between the tangential and z directions, and l_z is the z component of the atomic orbital angular momentum. Equation (12) describes four bands shifted in the Θ direction by $(l_z+\sigma/2)\varphi$, which depends on l and σ. The energy depends on $\Theta-(l_z+\sigma/2)\varphi$ that represents the momentum of the hopping motion. As illustrated in Fig. 6(a) (upper panel), $\sigma=1$ and $\sigma=-1$ bands are separated by $\Delta\Theta_S=\varphi$, whereas $l=1$ and $l=-1$ bands are separated by $\Delta\Theta_L = 2\varphi\cos\theta$.

The four bands with $\sigma=\pm1$ and $l=\pm1$ have four intersections between opposite-spin bands in the vicinity of $\Theta\sim\varphi\ll1$ as seen in Fig. 6(a) (upper panel). In particular, two intersections (⇳ in the figure) appear at nonzero Θ between same-l bands. Since Θ is nonzero at these intersections, spin splitting can occur with the time-reversal symmetry. The SOI-induced spin splitting is proportional to $|\langle\uparrow|\hat{\sigma}_{\hat{t}n}|\downarrow\rangle| = \sin\theta$, which is nonzero except at $\kappa=0$.

2. At $\tau \ll \kappa, \varphi \ll 1$ in type II region

When we assume $\tau \ll \kappa$ in addition to $\varphi \ll 1$, approximate solutions at $\Theta \sim \varphi$ are

$$|\mathrm{p}_{\hat{n}}\sigma\Theta\rangle,\ E_{\hat{n}\sigma}(\Theta) = 2\Big[V_\pi - \frac{(\kappa d)^2}{4}(V_\pi+V_\sigma)\Big]\cos\Big(\Theta-\frac{\sigma}{2}\varphi\Big), \quad (14)$$

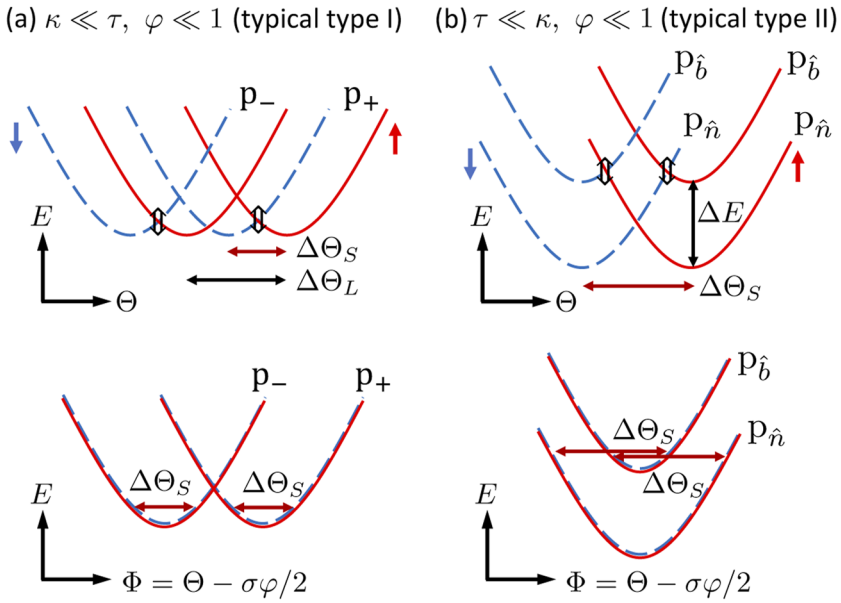

FIG. 6. Energy in the absence of the SOI is schematically shown in the upper panels as a function of Θ in the vicinity of $\Theta \sim \varphi \ll 1$. The spin splitting in the Θ direction, $\Delta\Theta_S = \varphi$, appears between $\sigma = \uparrow$ (solid line) and $\sigma = \downarrow$ (dashed line). (a) At $\kappa \ll \tau$ and $\varphi \ll 1$ (a typical type I region studied in Sec. III B 1), $p_\pm$ bands for each spin are relatively shifted by $\Delta\Theta_L = 2\varphi\cos\theta$ with θ the angle between the tangential and z directions. The SOI opens an energy gap at $\Updownarrow$ between same-orbital opposite-spin channels and gives rise to the spin-velocity locking. (b) At $\tau \ll \kappa$ and $\varphi \ll 1$ (a typical type II region studied in Sec. III B 2), $p_\pm$ bands are hybridized to $p_{\hat{n}}$ and $p_{\hat{b}}$ bands with energy splitting ΔE at the band bottom. The SOI opens a gap at $\Updownarrow$ between different-orbital opposite-spin channels. Also plotted in the lower panels are the energy as a function of the orbital component $\Phi = \Theta - \sigma\varphi/2$ obtained by subtracting the spin component $\sigma\varphi/2$.

$$|p_{\hat{b}}\sigma\Theta\rangle,\ E_{\hat{b}\sigma}(\Theta) = 2V_\pi \cos\left(\Theta - \frac{\sigma}{2}\varphi\right). \tag{15}$$

As illustrated in Fig. 6(b) (upper panel), $\sigma = 1$ and $\sigma = -1$ bands are separated by $\Delta\Theta_S = \varphi$, whereas $p_{\hat{n}}$ and $p_{\hat{b}}$ bands are separated in the energy direction by $\Delta E = (\kappa d)^2(V_\pi + V_\sigma)/2$ at the band bottom.

Again, two intersections ($\Updownarrow$ in the figure) appear at nonzero Θ between opposite-spin bands. In this case, the intersections at nonzero Θ are between different-orbital bands. For a gap to open at these intersections by the infinitesimal SOI, velocity directions of crossing channels must be opposite. This condition is satisfied when $E_{\hat{b}\uparrow}(\varphi/2) < E_{\hat{n}\downarrow}(\varphi/2)$, which leads to the inequality with V_σ/V_π, κd, and τd. In particular, at $\tau = 0$, the inequality becomes $(\kappa d)^2 > 2(3V_\pi + V_\sigma)/(V_\pi + V_\sigma)$. In carbon chains with $V_\sigma/V_\pi = -2.50$, this inequality shows that the type-II locking occurs at $\kappa > 0$ when $\tau = 0$. On the other hand, in iodine chains with $V_\sigma/V_\pi = -4.15$, the inequality leads to $\kappa d > 0.86$ as a requirement for the type-II locking to occur at $\tau = 0$. Although the approximation for $\varphi \ll 1$ is not applicable to the value of $\kappa d = 0.86$, the type-II locking region of iodine shown in Fig. 5 appears above almost the same threshold of κd at $\tau = 0$.

C. Origin of the spin-velocity locking

In Sec. III B, we have shown in the case of a large helix with $\varphi \ll 1$ that both the type-I locking at $\kappa \ll \tau$ and the type-II locking at $\tau \ll \kappa$ occur in the presence of the separation between opposite-spin bands $\Delta\Theta_S$. We show in this section that $\Delta\Theta_S$ is the origin of spin-velocity locking in our model.

In the presence of the helical symmetry, a linear combination of the spin $\sigma/2$ and the orbital component Φ, $\Theta = \sigma\varphi/2 + \Phi$, is conserved. Using Θ, the energy band with band index ν is described by $E_\nu(\Theta)$. In the absence of the SOI, the energy depends only on Φ and is expressed as $f(\Phi)$. Therefore, the energy as a function of Θ is given by $E_\nu(\Theta) = f(\Phi) = f(\Theta - \sigma\varphi/2)$ and opposite-σ bands are separated by $\Delta\Theta_S = \varphi$. This separation $\Delta\Theta_S$ generally creates intersections between opposite-σ channels. The opposite-σ states at the intersecting point $\Theta(=\sigma\varphi/2 + \Phi)$ have different Φ and, in most cases, have different velocities. When these velocities are opposite, the SOI opens an energy gap at the intersection, which can lead to the spin-velocity locking. Since spin-velocity locking derived in this paper originates from $\Delta\Theta_S$ in the presence of helical symmetry, we expect that the present spin-velocity locking occurs in a wide variety of helical structures.

The gap opening described above is analogous to the bandgap formation at the Brillouin zone boundary. To show this, we express the SOI [Eq. (6)] as

$$\hat{H}_{\rm so} = \sum_{l\Phi}\sum_{l'\Phi'} |p_{l'}\Phi'\rangle\langle p_{l'}\Phi'|\hat{H}_{\rm so}|p_l\Phi\rangle\langle p_l\Phi|, \tag{16}$$

by choosing basis vectors

$$|p_l\Phi\rangle = \frac{1}{\sqrt{N}}\sum_n \exp(i\Phi n)|p_l n\rangle. \tag{17}$$

Since $\hat{\sigma}_{\hat{t}n}$ in the intra-atomic SOI [Eq. (6)] is written as

$$\hat{\sigma}_{\hat{t}n} = (-i)\boldsymbol{e}_y \cdot \boldsymbol{e}_{\hat{t}0} \exp(-in\varphi)|\uparrow\rangle\langle\downarrow| + \text{h.c.} + \boldsymbol{e}_z \cdot \boldsymbol{e}_{\hat{t}0}\hat{\sigma}_z, \tag{18}$$

with $\boldsymbol{e}_y = (0,1,0)$, we obtain the following expression of the SOI,

$$\hat{H}_{\text{so}} = \frac{\lambda_{\text{so}}}{2}\sum_{l\Phi} l\big[\boldsymbol{e}_y \cdot \boldsymbol{e}_{\hat{t}0}(-i|\mathrm{p}_l\Phi - \varphi\rangle|\uparrow\rangle\langle\downarrow|\langle \mathrm{p}_l\Phi| + \text{h.c.}) + \boldsymbol{e}_z \cdot \boldsymbol{e}_{\hat{t}0}|\mathrm{p}_l\Phi\rangle\hat{\sigma}_z\langle \mathrm{p}_l\Phi|\big]. \tag{19}$$

Then, we find that the SOI mixes spin-$\downarrow$ Φ state and spin-$\uparrow$ $\Phi - \varphi$ $(=\Phi - \Delta\Theta_S)$ state. When these states have the same energy and the opposite velocity as shown in Fig. 6 (lower panels), a gap opens there. Thus, the present gap opening corresponds to the bandgap formation at the Brillouin zone boundary in which the periodic potential, through the Bragg reflection, mixes k $(=\pi/a)$ state and $k - G$ $(=-k)$ state to form standing waves, where $G = 2\pi/a$ and a is the lattice constant.

D. Comparison with previous theories

First, we compare our theory with the corresponding part of the theory by Utsumi *et al.*[15] They have considered a helical atomic chain that has an integer number of atoms per pitch ($2\pi/\varphi$ = integer). Helical atomic chains considered in this paper include both a chain with $2\pi/\varphi$ = integer and that with $2\pi/\varphi \neq$ integer. Utsumi *et al.*[15] have derived the SOI-induced spin flip accompanied by the momentum change [shown in Eq. (68) and illustrated in Fig. 6(a) of Ref. 15 in which k/N corresponds to Φ in Eq. (19) of this paper], which is equivalent to that derived in Eq. (19). They have presented the energy band structure at $\tau = 0$ in their model of hopping matrix elements, which shows degeneracy of $\mathrm{p}_{\hat{n}}$ and $\mathrm{p}_{\hat{b}}$ bands in the absence of the SOI. Then, the SOI opens a gap by mixing different-orbital opposite-spin states. Therefore, the resulting spin-velocity locking is type II. The degeneracy of $\mathrm{p}_{\hat{n}}$ and $\mathrm{p}_{\hat{b}}$ bands also takes place in our model by choosing $V_\pi = -V_\sigma$, $\tau = 0$, and $\lambda_{\text{so}} = 0$. In this case, we confirm in Fig. 7(b) that the SOI opens a gap at $\Theta = 0$. This can be regarded as the limit of $V_\pi \to -V_\sigma$ in the type II locking of our model, in which the SOI opens the gap by mixing different-orbital opposite-spin states as shown in Fig. 7(a) in the case of $V_\pi \neq -V_\sigma$.

Spin-velocity locking in the helical tube model by Michaeli and Naaman,[13] on the other hand, is type I since SOI opens a gap at the intersection between same-orbital opposite-spin channels. They have studied the case where the tube radius is much smaller than the radius and the pitch of the helix and derived approximate eigenstates that are, at the same time, eigenstates of the tangential component of the orbital angular momentum. The derived approximate eigenstates correspond to those in a typical type I region ($\mathrm{p}_\pm$ states at $\kappa \ll \tau$ and $\varphi \ll 1$) in our helical atomic chain, which are derived in Eq. (11) and illustrated in Fig. 6(a) (upper panel). In fact, their energy band structure has a close similarity to that shown schematically in Fig. 6(a) (upper panel), except for a quantitative difference in $\Delta\Theta_L$: $\Delta\Theta_L = 2\cos\theta\,\Delta\Theta_S$ in Eq. (12) of this paper, whereas $\Delta\Theta_L = 4\pi\cos\theta\,\Delta\Theta_S$ in Fig. 2(b) of Ref. 13.

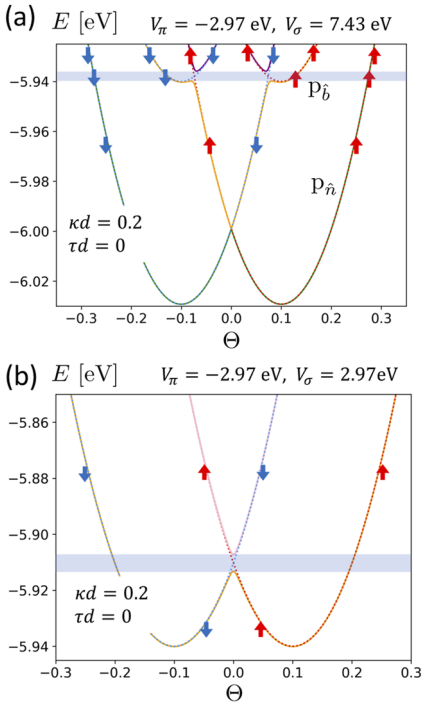

FIG. 7. Energy as a function of Θ at $\lambda_{\text{so}} = 0.006$ eV (solid lines) and $\lambda_{\text{so}} = 0$ (dotted lines) at $\kappa d = 0.2$ and $\tau d = 0$ for values of hopping parameters (a) $V_\pi = -2.97$ eV and $V_\sigma = 7.43$ eV corresponding to carbon and (b) $V_\pi = -V_\sigma = -2.97$ eV. When $V_\pi = -V_\sigma$, $\mathrm{p}_{\hat{n}}$ and $\mathrm{p}_{\hat{b}}$ bands become degenerate in the absence of the SOI.

IV. CONCLUSIONS

We have theoretically investigated electronic states in a helical chain of atomic $\mathrm{p}_\pm$ orbitals as a function of the curvature and the torsion of the helix. We have shown that spin-velocity locking in this system is classified into type I and type II, which occurs because an energy gap opens at the intersection between same-orbital channels and between different-orbital channels, respectively. In both types, the gap opens because the SOI mixes opposite-spin opposite-velocity states. This SOI-induced spin–flip reflection eliminates one transport channel for each spin so that each spin propagates in one direction within the gap. We have found that the velocity change associated with the spin flip in the SOI-induced spin–flip reflection is ensured by the helical symmetry in which a quantity consisting of spin and orbital components is conserved. Therefore, we expect that spin-velocity locking occurs in a wide variety of helical structures. In fact, it has been shown theoretically[25] that spin-velocity locking occurs in a helical model system for carbon nanotubes wrapped with DNA molecules, in which the spin selectivity has been theoretically predicted[26] and subsequently been experimentally confirmed.[27] In addition, the same paper[25] has shown that twisting a zigzag nanotube can induce the spin-velocity locking.

Finally, we compare the spin selectivity due to spin-velocity locking derived in this paper with the CISS in experiments. The

CISS has been observed at room temperature for which the thermal energy k_BT is ~30 meV. On the other hand, the SOI-induced energy gap at avoided crossing (Fig. 2) is ~3 meV in a carbon chain. Since spin-velocity locking is effective only for electrons within this energy gap, the spin-selectivity efficiency demonstrated in Fig. 3 will be reduced by an order of magnitude in the experimental situation where the current is carried by electrons in energy width of k_BT at room temperature. This suggests that to explain the CISS within the present model, we need to take into account additional effects such as electron-electron interaction, electron–phonon interaction, and proximity interaction with magnetized metal.[28] However, the present spin-velocity locking, which occurs in a nonmagnetic one-dimensional system, will be in itself worthwhile exploring even if it occurs only in the low temperature region.

ACKNOWLEDGMENTS

This work was supported by Grant-in-Aid for Scientific Research (C) Grant No. JP21K03413 from the Japan Society for the Promotion of Science (JSPS).

AUTHOR DECLARATIONS

Conflict of Interest

The authors have no conflicts to disclose.

Author Contributions

Shinnosuke Kashiwa: Conceptualization (supporting); Data curation (lead); Formal analysis (equal); Investigation (equal); Methodology (equal); Validation (equal); Visualization (lead); Writing – original draft (supporting); Writing – review & editing (supporting). **Hiroshi Akera**: Conceptualization (lead); Formal analysis (equal); Funding acquisition (lead); Investigation (equal); Methodology (equal); Project administration (lead); Supervision (lead); Validation (equal); Visualization (supporting); Writing – original draft (lead); Writing – review & editing (lead).

DATA AVAILABILITY

The data that support the findings of this study are available within the article.

APPENDIX: PROCEDURES TO CALCULATE EIGENSTATE ENERGY, GROUP VELOCITY, AND SPIN EXPECTATION VALUE

In this appendix we describe procedures to derive eigenstates of the Hamiltonian, $\hat{H}$, in Eq. (4), which express states of an electron traveling through a helical chain of atomic $p_\pm$ orbitals. We write each eigenvector $|\psi\rangle$ of $\hat{H}$ in a linear combination of basis vectors in Eq. (2), $|p_\alpha\sigma\Theta\rangle$ ($\alpha = \hat{n}, \hat{b}$, $\sigma = \pm 1$), which form a complete set of the present model with two orbitals, $p_{\hat{n}}$ and $p_{\hat{b}}$ in each atom:

$$|\psi\rangle = \sum_{\alpha\sigma\Theta} C_{\alpha\sigma\Theta}|p_\alpha\sigma\Theta\rangle. \tag{A1}$$

Owing to the helical symmetry with $\hat{S}^{-1}\hat{H}\hat{S} = \hat{H}$, we have

$$\langle p_{\alpha'}\sigma'\Theta'|(\hat{S}^{-1}\hat{H}\hat{S} - \hat{H})|p_\alpha\sigma\Theta\rangle = \langle p_{\alpha'}\sigma'\Theta'|\hat{H}|p_\alpha\sigma\Theta\rangle\left[\exp(i\Theta' - i\Theta) - 1\right] = 0. \tag{A2}$$

This leads to

$$\langle p_{\alpha'}\sigma'\Theta'|\hat{H}|p_\alpha\sigma\Theta\rangle = 0 \quad \text{when} \quad \Theta' \neq \Theta, \tag{A3}$$

i.e., the Hamiltonian matrix, $\langle p_{\alpha'}\sigma'\Theta'|\hat{H}|p_\alpha\sigma\Theta\rangle$, is diagonal in Θ. For each value of Θ, by diagonalizing 4×4 matrix, $\langle p_{\alpha'}\sigma'\Theta|\hat{H}|p_\alpha\sigma\Theta\rangle$, we obtain four eigenstates labeled by band index ν. Obtained eigenvalues $E_\nu(\Theta)$ of $\hat{H}$ are plotted as a function of Θ in Fig. 2 (upper panel). The group velocity along the helix axis of each eigenstate is given by $\frac{b\varphi}{\hbar}\frac{\partial E_\nu}{\partial\Theta}$. The eigenvector $|\nu\Theta\rangle$ is used to calculate the spin expectation value, $\langle\nu\Theta|\hat{\sigma}_z|\nu\Theta\rangle$, which is plotted in Fig. 2 (lower panel). In the absence of the SOI, the eigenstate of $\hat{H}$ is the eigenstate of $\hat{\sigma}_z$ with an eigenvalue, either of $\sigma = \pm 1$, and therefore the energy band with $\sigma = 1$ and that with $\sigma = -1$ cross (dotted lines in Fig. 2). In the presence of the SOI, these bands are mixed and an avoided crossing (also called anti-crossing) occurs (solid lines in Fig. 2).

REFERENCES

[1] S. G. Ray, S. S. Daube, G. Leitus, Z. Vager, and R. Naaman, "Chirality-induced spin-selective properties of self-assembled monolayers of DNA on gold," Phys. Rev. Lett. **96**, 036101 (2006).
[2] B. Göhler, V. Hamelbeck, T. Z. Markus, M. Kettner, G. F. Hanne, Z. Vager, R. Naaman, and H. Zacharias, "Spin selectivity in electron transmission through self-assembled monolayers of double-stranded DNA," Science **331**, 894–897 (2011).
[3] Z. Xie, T. Z. Markus, S. R. Cohen, Z. Vager, R. Gutierrez, and R. Naaman, "Spin specific electron conduction through DNA oligomers," Nano Lett. **11**, 4652–4655 (2011).
[4] D. Mishra, T. Z. Markus, R. Naaman, M. Kettner, B. Göhler, H. Zacharias, N. Friedman, M. Sheves, and C. Fontanesi, "Spin-dependent electron transmission through bacteriorhodopsin embedded in purple membrane," Proc. Natl. Acad. Sci. U. S. A. **110**, 14872–14876 (2013).
[5] M. Kettner, B. Göhler, H. Zacharias, D. Mishra, V. Kiran, R. Naaman, C. Fontanesi, D. H. Waldeck, S. Sęk, J. Pawłowski, and J. Juhaniewicz, "Spin filtering in electron transport through chiral oligopeptides," J. Phys. Chem. C **119**, 14542–14547 (2015).
[6] V. Kiran, S. P. Mathew, S. R. Cohen, I. Hernández Delgado, J. Lacour, and R. Naaman, "Helicenes—A new class of organic spin filter," Adv. Mater. **28**, 1957–1962 (2016).
[7] A. C. Aragonès, E. Medina, M. Ferrer-Huerta, N. Gimeno, M. Teixidó, J. L. Palma, N. Tao, J. M. Ugalde, E. Giralt, I. Díez-Pérez, and V. Mujica, "Measuring the spin-polarization power of a single chiral molecule," Small **13**, 1602519 (2017).
[8] M. Kettner, V. V. Maslyuk, D. Nürenberg, J. Seibel, R. Gutierrez, G. Cuniberti, K.-H. Ernst, and H. Zacharias, "Chirality-dependent electron spin filtering by molecular monolayers of helicenes," J. Phys. Chem. Lett. **9**, 2025–2030 (2018).
[9] S. Mishra, A. K. Mondal, S. Pal, T. K. Das, E. Z. B. Smolinsky, G. Siligardi, and R. Naaman, "Length-dependent electron spin polarization in oligopeptides and DNA," J. Phys. Chem. C **124**, 10776–10782 (2020).
[10] T. Liu, X. Wang, H. Wang, G. Shi, F. Gao, H. Feng, H. Deng, L. Hu, E. Lochner, P. Schlottmann, S. von Molnár, Y. Li, J. Zhao, and P. Xiong, "Linear and nonlinear two-terminal spin-valve effect from chirality-induced spin selectivity," ACS Nano **14**, 15983–15991 (2020).
[11] R. Naaman and D. H. Waldeck, "Spintronics and chirality: Spin selectivity in electron transport through chiral molecules," Annu. Rev. Phys. Chem. **66**, 263–281 (2015).

[12]A. Inui, R. Aoki, Y. Nishiue, K. Shiota, Y. Kousaka, H. Shishido, D. Hirobe, M. Suda, J.-I. Ohe, J.-I. Kishine, H. M. Yamamoto, and Y. Togawa, "Chirality-induced spin-polarized state of a chiral crystal $CrNb_3S_6$," Phys. Rev. Lett. **124**, 166602 (2020).
[13]K. Michaeli and R. Naaman, "Origin of spin-dependent tunneling through chiral molecules," J. Phys. Chem. C **123**, 17043–17048 (2019).
[14]S. Varela, V. Mujica, and E. Medina, "Effective spin-orbit couplings in an analytical tight-binding model of DNA: Spin filtering and chiral spin transport," Phys. Rev. B **93**, 155436 (2016).
[15]Y. Utsumi, O. Entin-Wohlman, and A. Aharony, "Spin selectivity through time-reversal symmetric helical junctions," Phys. Rev. B **102**, 035445 (2020).
[16]Y. Utsumi, T. Kato, O. Entin-Wohlman, and A. Aharony, "Spin-filtering in a *p*-orbital helical atomic chain," Isr. J. Chem. **62**, e202200107 (2022).
[17]R. Otsuto, Y. Yatabe, and H. Akera, "Orbital and spin polarizations induced by current through a helical atomic chain," Phys. Rev. B **104**, 035431 (2021).
[18]W. Izumida, K. Sato, and R. Saito, "Spin-orbit interaction in single wall carbon nanotubes: Symmetry adapted tight-binding calculation and effective model analysis," J. Phys. Soc. Jpn. **78**, 074707 (2009).
[19]T. Ando, "Spin-orbit interaction in carbon nanotubes," J. Phys. Soc. Jpn. **69**, 1757–1763 (2000).
[20]J. C. Slater and G. F. Koster, "Simplified LCAO method for the periodic potential problem," Phys. Rev. **94**, 1498–1524 (1954).
[21]M. S. Tang, C. Z. Wang, C. T. Chan, and K. M. Ho, "Environment-dependent tight-binding potential model," Phys. Rev. B **53**, 979–982 (1996).
[22]X. Zhao, Y. Ando, Y. Liu, M. Jinno, and T. Suzuki, "Carbon nanowire made of a long linear carbon chain inserted inside a multiwalled carbon nanotube," Phys. Rev. Lett. **90**, 187401 (2003).
[23]P. Carrier and S.-H. Wei, "Calculated spin-orbit splitting of all diamondlike and zinc-blende semiconductors: Effects of $p_{1/2}$ local orbitals and chemical trends," Phys. Rev. B **70**, 035212 (2004).
[24]D. Rybkovskiy, A. Osadchy, and E. Obraztsova, "Electronic band structure of helical iodine chains," Phys. Status Solidi B **249**, 2608–2611 (2012).
[25]Y. Perlitz and K. Michaeli, "Helical liquid in carbon nanotubes wrapped with DNA molecules," Phys. Rev. B **98**, 195405 (2018).
[26]G. S. Diniz, A. Latgé, and S. E. Ulloa, "Helicoidal fields and spin polarized currents in carbon nanotube–DNA hybrids," Phys. Rev. Lett. **108**, 126601 (2012).
[27]K. M. Alam and S. Pramanik, "Spin filtering through single-wall carbon nanotubes functionalized with single-stranded DNA," Adv. Funct. Mater. **25**, 3210–3218 (2015).
[28]J. Fransson, "The chiral induced spin selectivity effect what it is, what it is not, and why it matters," Isr. J. Chem. **62**, e202200046 (2022).